Adaptive Contextual Energy Parameterization for Automated Image Segmentation

Josna Rao[1], Ghassan Hamarneh[2], and Rafeef Abugharbieh[1]

[1] Biomedical Signal and Image Computing Lab,
University of British Columbia, Canada
[2] Medical Image Analysis Lab, Simon Fraser University, Canada
josnar@ece.ubc.ca, hamarneh@cs.sfu.ca, rafeef@ece.ubc.ca

Abstract. Image segmentation techniques are predominately based on parameter-laden optimization processes. The segmentation objective function traditionally involves parameters (i.e. weights) that need to be tuned in order to balance the underlying competing cost terms of image data fidelity and contour regularization. In this paper, we propose a novel approach for automatic adaptive energy parameterization. In particular, our contributions are three-fold; 1) We spatially adapt fidelity and regularization weights to local image content in an autonomous manner. 2) We modulate the weight using a novel contextual measure of image quality based on the concept of spectral flatness. 3) We incorporate our proposed parameterization into a general segmentation framework and demonstrate its superiority to two alternative approaches: the best possible spatially-fixed parameterization and the globally optimal spatially-varying, but non-contextual, parameters. Our segmentation results are evaluated on real and synthetic data and produce a reduction in mean segmentation error when compared to alternative approaches.

Keywords: Adaptive regularization, contextual weights, image segmentation, energy minimization, adapting energy functional, spectral flatness, noise estimation.

1 Introduction

Robust automated image segmentation is a highly sought after goal that continues to defy solution. In medical images, for example, natural and pathological variability as well as noise often result in unpredictable image and shape features that significantly complicate segmentation tasks. Furthermore, spatially nonuniform noise can result from numerous reconstruction and postprocessing techniques on MR images to correct for intensity inhomogeneity effects and from images obtained with decreased acquisition times and high speedup factors [1]. Current state-of-the-art segmentation methods are predominantly based on optimization procedures that produce so called 'optimal' segmentations at their minimum. The optimization methods typically incorporate a tradeoff between two classes of cost terms: data fidelity and contour regularization. This is the case not only in image segmentation, but also in image registration, shape matching,

G. Bebis et al. (Eds.): ISVC 2009, Part I, LNCS 5875, pp. 1089–1100, 2009.

and other computer vision tasks. This basic tradeoff scheme is ubiquitous, relating to Occam's razor and Akaike/Bayesian information criteria [2], and is seen in many forms, such as likelihood versus prior in Bayesian methods [3] and loss versus penalty in machine learning [4]. Making progress toward determining how to best control such balancing between competing cost terms within the optimization process is therefore of great importance to many related algorithmic formulations in computer vision as well as numerous applications most notably in medical image analysis. Examples of optimization-based segmentation methods that are fragile and highly sensitive to the aforementioned tradeoffs are plentiful, including active contours techniques [5][6][7][8], graph cut methods [9], and optimal path approaches [10].

For simplifying the exposition of the ideas in this paper, we will adopt the simplified but general form of the cost or energy function:

$$E(S|I, \alpha, \beta) = \alpha E_{int}(S) + \beta E_{ext}(S|I) \tag{1}$$

where S is the segmentation and I is the image. E_{int} is the internal cost term contributing to the regularization of the segmentation, most often by enforcing some smoothness constraints, in order to counteract the effects of imaging artifacts. E_{ext} is the external cost term contributing to the contour's conformity to desired image features, e.g. edges. The weights α and β are typically set empirically by the users based on their judgment of how to best balance the requirements for regularization and adherence to image content. In most cases, this is a very difficult task and the parameters may be unintuitive for a typical non-technical end user, e.g. a clinician, who lacks knowledge of the underlying algorithm's inner working. Also the resultant segmentations can vary drastically based on how this balance is set. Avoiding the practice of ad-hoc setting of such weights is the driving motivation for our work here.

To the best of our knowledge, regularization weights have traditionally been determined empirically and are fixed across the image domain (i.e. do not vary spatially). In Pluempitiwiriyawej *et al.* [8], the weights are changed *as the optimization progresses*, albeit in an ad-hoc predetermined manner. McIntosh and Hamarneh [11] demonstrated that adapting the regularization weights *across a set of images* is necessary in addressing the variability in real clinical image data. However, neither approach varies the weights spatially across the image and hence are not responsive or adaptive to local features within a single image.

Image regions with noise, weak or missing boundaries, and/or occlusions are commonly encountered in real image data. For example, degradation in medical images can occur due to tissue heterogeneity ("graded decomposition" [12]), patient motion, or imaging artifacts, e.g. echo dropouts in ultrasound or nonuniformity in magnetic resonance. In such cases and in order to increase segmentation robustness and accuracy, *more regularization is needed in less reliable image regions* which suffer from greater deterioration. Although an optimal regularization weight can be found for a single image in a set [11], the same weight may not be optimal for all regions of that image. Spatially adapting the regularization weights provides greater control over the segmentation result, allowing it

to adapt not only to images with spatially varying noise levels and edge strength, but also to objects with spatially-varying shape characteristics, e.g. smooth in some parts and jagged in others.

Some form of spatially adaptive regularization over a single image appeared in a recent work by Dong *et al.* [13]. For segmenting an aneurysm, they varied the amount of regularization based on the surface curvature of a *pre-segmented* vessel. The results demonstrated improvements due to adaptive regularization. However, the regularization weights did not rely on the properties of the image itself, which limited the generality of the method. Kokkinos *et al.* [14] investigated the use of adaptive weights for the task of separating edge areas from textured regions using a probabilistic framework, where the posterior probabilities of edge, texture, and smoothness cues were used as weights for curve evolution. Similarly, Malik *et al.* [15] and, very recently, Erdem and Tari [16] tackled the problem of texture separation and selected weights based on data cues. However, while these methods focused on curve evolution frameworks, our current work focuses on graph-based segmentation. Additionally, we emphasize balancing the cost terms by adapting the regularization for images plagued by nonuniform noise and weak or diffused edges rather than textured patterns in natural images.

In this paper, we advocate the strong need for spatially-adaptive balancing of cost terms in an automated, robust, data-driven manner to relax the requirement on the user to painstakingly tweak these parameters. We also demonstrate how existing fixed-weight approaches (even if globally optimized) are often inadequate for achieving accurate segmentation. To address the problem, we propose a novel data-driven method for spatial adaptation of optimization weights. We develop a new spectral flatness measure of local image noise to balance the energy cost terms at every pixel, without any prior knowledge or fine-tuning.

We validate our method on synthetic, medical, and natural images and compare its performance against two alternative approaches for regularization: using the best possible spatially-fixed weight, and using the globally optimal set of spatially-varying weights as found automatically through dynamic programming.

2 Methods

2.1 Energy-Minimizing Segmentation

Our formulation employs energy-minimizing boundary-based segmentation, where the objective is to find a contour that correctly separates an object from background. We embed a parametric contour $C(q) = C(x(q), y(q)) : [0, 1] \rightarrow \Omega \subset \mathbf{R^2}$ in image $I : \Omega \rightarrow \mathbf{R}$. We use a single adaptive weight $w(q) \in [0, 1]$ that varies over the length of the contour and re-write (1) as:

$$E(C(q), w(q)) = \int_0^1 (w(q)E_{int}(C(q)) + (1 - w(q))E_{ext}(C(q)))\, dq \qquad (2)$$

where

$$E_{ext}(C(q)) = 1 - |\nabla I(C(q))| \,/\, \max_{\Omega} |\nabla I(C(q))| \qquad (3)$$

penalizes weak boundaries and

$$E_{int}(C(q)) = |dC(q)/dq| \tag{4}$$

penalizes longer and more jagged contours. Sec. 2.4 discusses the discrete formulation to minimize E with respect to $C(q)$ in (2).

2.2 Spatially Adaptive Energy Parameterization

Our approach for balancing the cost terms is to gauge the levels of signal vs. noise in local image regions. We estimate the edge evidence $G(x, y)$ and noise level $N(x, y)$ in each region of the image and set $w(x, y)$ in (2) such that regions with high noise and low boundary evidence (i.e. low reliability) have greater regularization, and vice versa. Hence, image reliability $R(x, y) \in [0, 1]$ is mapped to $w(x, y)$ as

$$w(x, y) = 1 - R(x, y) \tag{5}$$

where

$$R(x, y) = (1 - N(x, y))\, G(x, y). \tag{6}$$

Assuming additive white noise, uncorrelated between pixels, we propose to estimate spatially-varying noise levels $N(x, y)$ using a local image spectral flatness (SF) measure. SF is a well-known Fourier-domain measure that has been employed in audio signal processing and compression applications [17][18]. SF exploits the property that white noise exhibits similar power levels in all spectral bands and thus results in a flat power spectrum, whereas uncorrupted signals have power concentrated in certain spectral bands and thus result in a more impulse-like power spectrum. In this paper, we extend the SF measure to 2D and measure $N(x, y)$ as

$$N(x, y) = \frac{\exp\left(\frac{1}{4\pi^2}\int_{-\pi}^{\pi}\int_{-\pi}^{\pi} \ln S\left(\omega_x, \omega_y\right) d\omega_x d\omega_y\right)}{\frac{1}{4\pi^2}\int_{-\pi}^{\pi}\int_{-\pi}^{\pi} S\left(\omega_x, \omega_y\right) d\omega_x d\omega_y} \tag{7}$$

where $S(\omega_x, \omega_y) = |F(\omega_x, \omega_y)|^2$ is the 2D power spectrum of the image, $F(\omega_x, \omega_y)$ is the Fourier spectrum of the image and (ω_x, ω_y) are spatial radian frequencies. Note that (7) can be easily extended to 3D images via a triple integral. We use $G(x, y) = \max\left(|\nabla I_x(x, y)|, |\nabla I_y(x, y)|\right)$, where $\nabla I_x(x, y)$ and $\nabla I_y(x, y)$ represent the x and y components of the image gradient. We chose this measure rather than the standard gradient magnitude for its rotational invariance in the discrete domain.

2.3 Non-contextual Globally Optimal Weights

A theoretically appealing and intuitive approach for setting the regularization weight is to optimize E in (2) for the *weight* $w(q)$ *itself* in addition to optimizing the contour. In our discrete setting, this involves a 'three dimensional'

graph search that computes the globally optimal, spatially-adaptive regularization weight $w(q)$, in conjunction with the contour's spatial coordinates, i.e. we optimize[1] $\tilde{C}(q) = (x(q), y(q), w(q))$. Sec. 2.4 discusses the method for implementing the graph search.

As we demonstrate later in Sec. 3, there are three main drawbacks to this globally optimum (in (x, y, w)) method: (i) it does not explicitly encode image reliability, even though regularization is essential in regions with low reliability; (ii) it encourages a bimodal behavior of the regularization weight (this is easy to observe as the weight will be allocated to whichever cost is smaller):

$$w(q) = \left\{ \begin{matrix} 0, & E_{int}(q) > E_{ext}(q) \\ 1, & \text{otherwise} \end{matrix} \right\}, \tag{8}$$

and (iii) it combines the weight and segmentation optimization into one process, thus reducing the generality of the method as finding globally-optimal weights for other segmentation frameworks would require significant changes to the energy minimization process. In short, even though *optimal* with respect to E in (2), the solution is *incorrect* and, as we later demonstrate, inferior to the spatially adaptive balancing of energy cost terms proposed in Sec. 2.2.

2.4 Implementation Details

To minimize E with respect to $C(q)$ in (2), we model the image as a graph where each pixel is represented by a vertex v_i in the graph, and graph edges $e_{ij} = \langle v_i, v_j \rangle$ capture the pixel's connectedness (e.g. 8-connectedness in 2D images). A local cost $c_{ij} = wE_{int}(v_i, v_j) + (1 - w)E_{ext}(v_i)$ is assigned to each edge e_{ij}, where $E_{int}(v_i, v_j)$ is the Euclidean distances between v_i and v_j (*e.g.* 1 for 4-connected neighbors and $\sqrt{2}$ for diagonal neighbors in 2D). The contour that minimizes the total energy $E = \sum_{e_{ij} \in C} c_{ij}$ represents the optimal solution for the segmentation and is found by solving a minimal path problem, e.g. the global snake minimization method between two end points presented in [21] which does not require any initialization other than specifying the end points.

The non-contextual globally optimal weight (Sec. 2.3) is determined through dynamic programming. In our formulation, each vertex in the original graph is now replaced by K vertices representing the different choices of the weight value at each pixel. In addition, graph edges now connect vertices corresponding to neighboring image pixels for all possible weights. Note that the optimal path $\tilde{C}(q) = (x(q), y(q), w(q))$ cannot pass through the same $(x(q), y(q))$ for different w, i.e. only a single weight can be assigned per pixel. Our graph search abides by this simple and logical constraint. The optimal $C(q)$ and $w(q)$ that globally minimize (2) are again calculated using dynamic programming but now on this new (x, y, w) graph.

[1] This is similar in spirit to [19] and [20] where they also optimize for a non-spatial variable: vessel radius or scale, in addition to the spatial coordinates of the segmentation contour.

To further demonstrate the global utility of our proposed contextual parameterization approach, we tested incorporating our adaptive weights into a traditional graph cuts (GC) segmentation framework [22][23], where the segmentation energy is

$$E(f) = \sum_{p,q \in N} V_{p,q}(f_p, f_q) + \sum_{p \in P} D_p(f_p). \tag{9}$$

$f \in \mathcal{L}$ is the labeling for all pixels $p \in P$ where $\mathcal{L}$ is the label space and P is the set of pixels in image I. $V_{p,q}$ is the pairwise interaction penalty between pixel pairs (i.e. the penalty of assigning labels f_p and f_q to pixels p and q), N is the set of interacting pairs of pixels, and D_p measures how well label f_p fits pixel p given the observed data. D_p is calculated as the difference in intensity between pixel p and the mean intensity of seeds within label f_p, and the interaction penalty is calculated as $V_{p,q} = e^{-|\nabla I(x,y)|^2}$ such that low gradient magnitude regions have a high interaction penalty. We modified this standard GC optimization process by replacing $V_{p,q}$ by our proposed spatially adaptive weight in (5).

3 Results and Discussion

We first performed quantitative tests on 16 synthetic images carefully designed to cover extreme shape and appearance variations (two examples are shown in Fig. 1). We created the test data by modeling an object boundary as a sinusoidal function with spatially-varying frequency to simulate varying contour smoothness conditions, and we added spatially-varying (non-stationary) additive white Gaussian noise patterns of increasing variance. We also spatially varied the gradient magnitude of the object boundary across each image by applying Gaussian blurring kernels at different scales in different locations. Computationally, the proposed method required less than 5 minutes for a 768×576 image when run on a Pentium 4 (3.6GHz) machine using MATLAB code.

Our resulting image reliability measure is exemplified in Fig. 1 for two synthetic images with the resulting segmentations shown in Fig. 2. The contour obtained using the globally-optimal weights method (Sec. 2.3) is also shown, along with the contour obtained using a *spatially-fixed* regularization weight, set to the value producing *the smallest* (via brute force search) segmentation error.

We quantitatively examined our method's performance using ANOVA testing on 25 noise realizations of each image in the dataset, where the error was determined by the Hausdorff distance to the ground truth contour. Our method resulted in a mean error (in pixels) of 6.33 ± 1.36, whereas the best fixed-weight method had a mean error of 12.05 ± 1.61, and the globally-optimum weight method had a mean error of 33.06 ± 3.66. Furthermore, for each image, we found our method to be significantly more accurate with all p-values $<< 0.05$.

We also tested our method on clinical MR images of the corpus callosum (CC), which exhibits the known problem of a weak boundary where the CC meets the fornix (Fig. 3(a)). Note how the contour obtained using globally optimal weights exhibits an optimal, yet undesirable, bimodal behavior (either blue

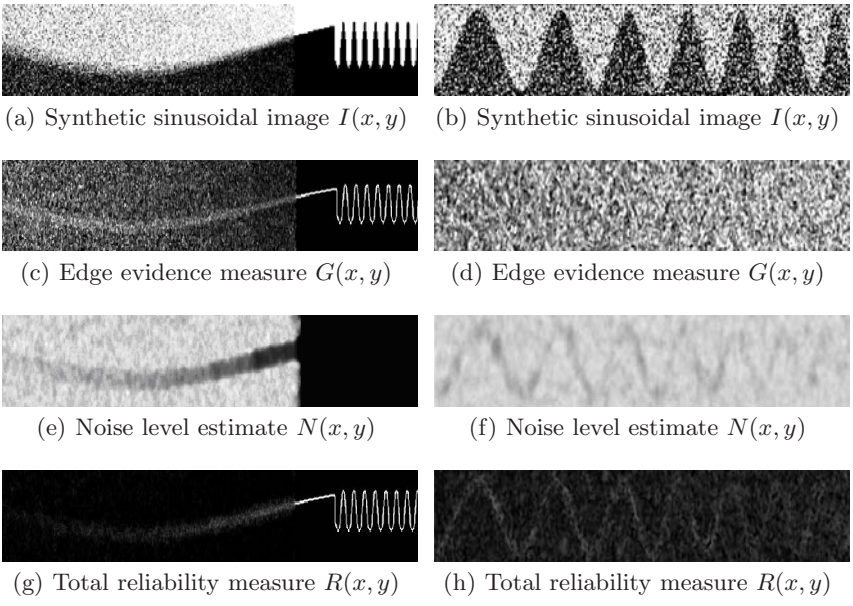

(a) Synthetic sinusoidal image $I(x, y)$ (b) Synthetic sinusoidal image $I(x, y)$

(c) Edge evidence measure $G(x, y)$ (d) Edge evidence measure $G(x, y)$

(e) Noise level estimate $N(x, y)$ (f) Noise level estimate $N(x, y)$

(g) Total reliability measure $R(x, y)$ (h) Total reliability measure $R(x, y)$

Fig. 1. Two sample synthetic images used in our validation tests. The left column image has spatially varying noise and blurring (increasing from right to left) and with changing boundary smoothness (smooth on the left and jagged on the right). The right column image has higher curvature and noise levels. Black intensities corresponds to 0 and white to 1. The result confirms the desired behavior of the reliability measure.

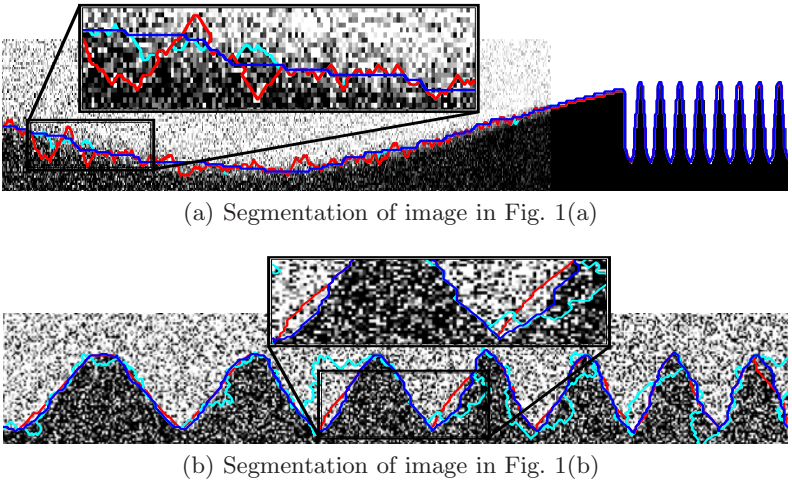

(a) Segmentation of image in Fig. 1(a)

(b) Segmentation of image in Fig. 1(b)

Fig. 2. *Color is essential for proper viewing, please refer to the e-copy.* Contours obtained from: (*blue*) proposed adaptive weights, (*red*) best fixed weight, and (*cyan*) globally optimum weight.

or red in Fig. 3(a)) completely favoring only one of the terms at a time. In comparison, our method automatically boosts up the regularization (stronger red in Fig. 3(b)) at the CC-fornix boundary producing a better delineation, as seen in the segmentation results (Fig. 3(c)).

In addition, we tested our method on MR data from BrainWeb [24]. Fig. 4 shows the segmentation of the cortical surface in a proton density (PD) image with a noise level of 5%. This example is a difficult scenario due to the high level of noise and low resolution of the image. The proposed method provided a smoother contour while conforming to the cortical boundary when compared to the other methods (although the difference was not too large).

To demonstrate the general applicability of our method, we also used natural images in our testing, such as the tree leaf on a complicated background shown in Fig. 5(a). The resulting reliability measure (Fig. 5(b)) has lower image reliability

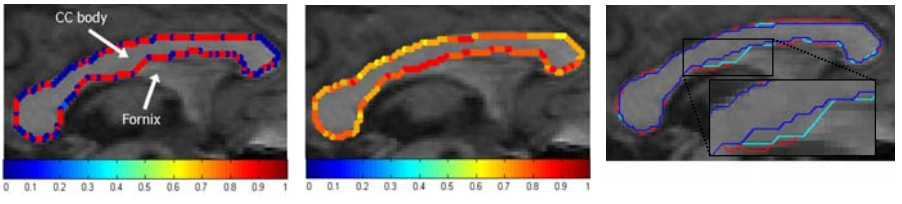

(a) (b) (c)

Fig. 3. (*Color figure, refer to e-copy*). Results of (a) globally-optimum weight method and (b) proposed adaptive-weight method for a corpus callosum MR image. The coloring of the contours reflects the value of the spatially-adaptive weight. The same color map is used for both figures, with pure blue corresponding to $w = 0$ and pure red to $w = 1$. The proposed method results in greater regularization in the difficult fornix region and has smoother transition between weights. (c) Contours produced by using the proposed adaptive weight (*blue*), best fixed-weight (*red*), and the globally-optimum weight (*cyan*).

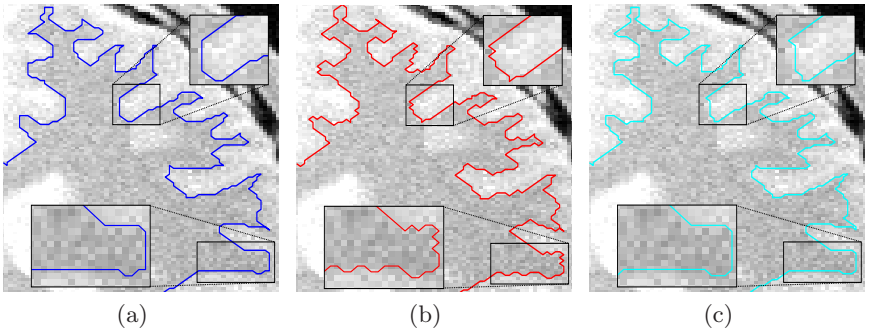

(a) (b) (c)

Fig. 4. (*Color figure, refer to e-copy*). Segmentation results on BrainWeb data of cortical surface in a proton density image with noise level of 5%. Contours produced by using (a) the proposed adaptive weight (*blue*), (b) best fixed-weight (*red*), and (c) the globally-optimum weight (*cyan*). Improved regularization resulted from our method.

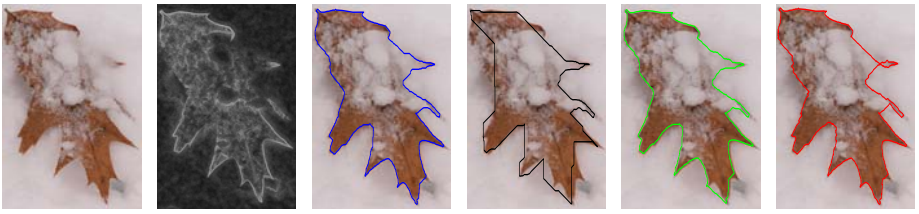

Fig. 5. (*Color figure, refer to e-copy*). Segmenting a natural image. (a) Original leaf image. (b) Reliability calculated by our proposed method. Contours produced by using (c) our method (*blue*), (d) fixed-weight of 1 (*black*), (e) 0.5 (*green*), and (f) 0 (*red*).

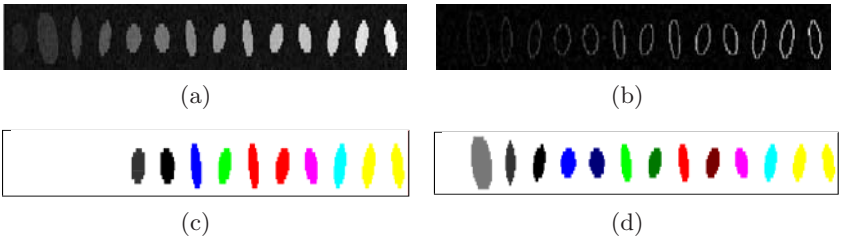

Fig. 6. (*Color figure, refer to e-copy*). Segmentation of a synthetic image using GC with adaptive regularization. (a) Synthetic image of 14 ellipses with image contrast increasing from left to right. (b) Reliability calculated by our proposed method. (c) Segmentation using standard GC, where each color represents a separate label. (d) Segmentation using adaptive regularization GC.

and, hence, higher regularization at the regions of the leaf obscured by snow, whereas reliable boundaries light up (bright white boundary segments). The resulting segmentations are shown in Figs. 5(c) to 5(f) (note that no best-fixed weight was determined since a true segmentation of the image is not known).

We validated Graph Cuts with our proposed method on simulated noisy images of variably-sized ellipses with complicated background patterns, e.g. with image contrast decreasing from right to left, as in Fig. 6(a). The leftmost ellipses with lower contrast have a lower SNR than the rightmost ellipses and thus require greater regularization. Note how our resulting reliability measure (Fig. 6(b)) indicates lower image reliability for low contrast ellipses. When comparing our segmentation results to those of standard GC (Sec. 2.4), as shown in Fig. 6(c), 6 ellipses out of 14 were mislabeled, whereas GC with adaptive regularization correctly labeled 12 ellipses (Fig. 6(d)). To quantify the advantage of our approach, we tested a synthetic dataset of images containing 2 to 40 ellipses at various noise levels. We calculated the Dice similarity coefficient (DSC) of the segmentation to the ground truth for each ellipse and averaged over all the ellipses in the image. Fig. 7 plots the difference in average DSC between adaptive regularization GC and standard GC for images of increasing ellipse numbers.

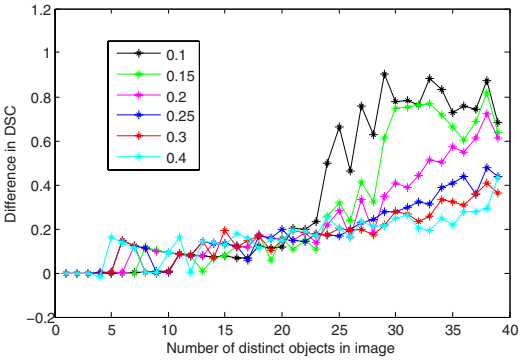

Fig. 7. (*Color figure, refer to e-copy*). Difference in average DSC between adaptive regularization GC and standard GC for images with increasing numbers of ellipses. Different curves represent different noise standard deviations as shown in legend. Positive DSC difference indicates adaptive regularization GC is more successful than standard GC at labeling ellipses with low image quality.

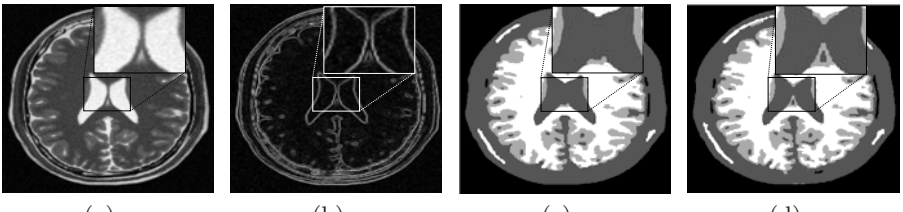

Fig. 8. Segmentation of MR data from BrainWeb using GC with adaptive regularization. (a) Original T2 slice with 3% noise level and 40% intensity non-uniformity. (b) Reliability calculated by our proposed method. Note increased reliability along the ventricular boundary. (c) Segmentation from standard GC. (d) Segmentation from GC with adaptive regularization.

The same images were also tested at various noise levels. Note that a positive difference in the DSC indicates that our proposed regularization method with GC had greater success detecting low contrast ellipses.

Finally, we tested Graph Cuts with our proposed method on MR data from BrainWeb [24] using a low number of seeds (0.1% of image pixels for each label). Fig. 8(a) shows a T2 image with a noise level of 3% and an intensity non-uniformity of 40%. Increased reliability along the ventricle boundary (Fig. 8(b)) results in lower regularization and greater accuracy in the adaptive regularization GC result (Fig. 8(d)) when compared to the standard GC result (Fig. 8(c)) for a segmentation of the ventricles and cortical surface.

4 Conclusion

We proposed a novel approach for addressing a ubiquitous problem that plagues most energy minimization based segmentation techniques; how to properly balance the weights of competing data fidelity and regularization energy terms. Our technique spatially adapts the regularization weight based on a novel measure of image data reliability. The proposed spectral flatness metric reflects the spatially-varying evidence of signal versus noise and is automatically derived without any tuning. We incorporated our proposed contextual parameterization technique into a general segmentation framework and demonstrated its superiority to non-contextual parameterization even when the latter employed globally optimized values of the objective function parameters. Using quantitative and qualitative tests, we demonstrated that regularization needs to vary spatially and must increase where image evidence is less reliable. Our simple approach is powerful and was shown to be capable of handling varying image data ranging from MRI scans to natural images. Additionally, we demonstrated our approach's general applicability in that it can be extended to state-of-the-art energy-minimization segmentation frameworks such as Graph Cuts.

We are currently extending our approach to other variational and graph-based segmentation approaches such as [5][25]. Additionally, we intend to expand our technique to handle energy functionals where multiple weights balance the different energy terms and to explore alternative image reliability metrics. Another important conclusion of our findings is that globally optimal weights do not necessarily reflect correct segmentations. We intend to further explore this issue and its implications in more detail.

References

1. Samsonov, A.A., Johnson, C.R.: Noise-adaptive nonlinear diffusion filtering of MR images with spatially varying noise levels. Magnetic Resonance in Medicine 52(4), 798–806 (2004)
2. Burnham, K.P., Anderson, D.R.: Multimodel inference: Understanding AIC and BIC in model selection. Sociological Methods & Research 33(2), 291–304 (2004)
3. Akselrod-Ballin, A., Galun, M., Gomori, M.J., Brandt, A., Basri, R.: Prior knowledge driven multiscale segmentation of brain MRI. In: Ayache, N., Ourselin, S., Maeder, A. (eds.) MICCAI 2007, Part II. LNCS, vol. 4792, pp. 118–126. Springer, Heidelberg (2007)
4. Zhao, P., Yu, B.: Stagewise lasso. Journal of Machine Learning Research 8, 2701–2726 (2007)
5. Kass, M., Witkin, A., Terzopoulos, D.: Snakes: Active contour models. International Journal of Computer Vision 1(4), 321–331 (1988)
6. Caselles, V., Kimmel, R., Sapiro, G.: Geodesic active contours. International Journal of Computer Vision 22(1), 61–79 (1997)
7. Osher, S.J., Paragios, N.: Geometric Level Set Methods in Imaging, Vision, and Graphics. Springer, Heidelberg (2003)
8. Pluempitiwiriyawej, C., Moura, J.M.F., Wu, Y.J.L., Ho, C.: STACS: New active contour scheme for cardiac MR image segmentation. IEEE Transactions on Medical Imaging 24(5), 593–603 (2005)

9. Boykov, Y., Funka-Lea, G.: Graph cuts and efficient N-D image segmentation. Int. J. Comput. Vision 70(2), 109–131 (2006)
10. Barrett, W.A., Mortensen, E.N.: Interactive live-wire boundary extraction. Medical Image Analysis 1, 331–341 (1997)
11. McIntosh, C., Hamarneh, G.: Is a single energy functional sufficient? Adaptive energy functionals and automatic initialization. In: Ayache, N., Ourselin, S., Maeder, A. (eds.) MICCAI 2007, Part II. LNCS, vol. 4792, pp. 503–510. Springer, Heidelberg (2007)
12. Udupa, J.K., Grevera, G.J.: Go digital, go fuzzy. Pattern Recognition Letters 23(6), 743–754 (2002)
13. Dong, B., Chien, A., Mao, Y., Ye, J., Osher, S.: Level set based surface capturing in 3D medical images. In: Metaxas, D., Axel, L., Fichtinger, G., Székely, G. (eds.) MICCAI 2008, Part I. LNCS, vol. 5241, pp. 162–169. Springer, Heidelberg (2008)
14. Kokkinos, I., Evangelopoulos, G., Maragos, P.: Texture analysis and segmentation using modulation features, generative models, and weighted curve evolution. IEEE Trans. Pattern Analysis and Machine Intelligence 31(1), 142–157 (2009)
15. Malik, J., Belongie, S., Leung, T.K., Shi, J.: Contour and texture analysis for image segmentation. International Journal of Computer Vision 43(1), 7–27 (2001)
16. Erdem, E., Tari, S.: Mumford-Shah regularizer with contextual feedback. Journal of Mathematical Imaging and Vision 33(1), 67–84 (2009)
17. Jayant, N.S., Noll, P.: Digital Coding of Waveforms. Prentice-Hall, Englewood Cliffs (1984)
18. Taubman, D.S., Marcellin, M.W.: JPEG 2000: Image Compression Fundamentals, Standards and Practice. Kluwer Academic Publishers, Norwell (2001)
19. Poon, K., Hamarneh, G., Abugharbieh, R.: Live-vessel: Extending livewire for simultaneous extraction of optimal medial and boundary paths in vascular images. In: Ayache, N., Ourselin, S., Maeder, A. (eds.) MICCAI 2007, Part II. LNCS, vol. 4792, pp. 444–451. Springer, Heidelberg (2007)
20. Li, H., Yezzi, A.: Vessels as 4-D curves: Global minimal 4-D paths to extract 3-D tubular surfaces and centerlines. IEEE Transactions on Medical Imaging 26(9), 1213–1223 (2007)
21. Cohen, L.D., Kimmel, R.: Global minimum for active contour models: A minimal path approach. International Journal of Computer Vision 24(1), 57–78 (1997)
22. Bagon, S.: Matlab wrapper for graph cut (December 2006)
23. Boykov, Y., Veksler, O., Zabih, R.: Fast approximate energy minimization via graph cuts. IEEE transactions on Pattern Analysis and Machine Intelligence 20(12), 1222–1239 (2001)
24. Cocosco, C.A., Kollokian, V., Kwan, R.K.S., Evans, A.C.: BrainWeb: Online interface to a 3D MRI simulated brain database. In: Friberg, L., Gjedde, A., Holm, S., Lassen, N.A., Nowak, M. (eds.) Third International Conference on Functional Mapping of the Human Brain, NeuroImage, vol. 5. Academic Press, London (1997)
25. Chan, T.F., Vese, L.A.: Active contours without edges. IEEE Transactions on Image Processing 10(2), 266–277 (2001)